IEEE Access
Multidisciplinary | Rapid Review | Open Access Journal

Received April 14, 2021, accepted April 22, 2021, date of publication April 30, 2021, date of current version May 17, 2021.

Digital Object Identifier 10.1109/ACCESS.2021.3076926

A Double-Veined Leaf-Shaped Bionic Meta-Element and Array Loading Antennas for Radiation Beam Control

BAIQIANG YOU, (Senior Member, IEEE), YONGCHUN OU, JINGLIN YOU, AND HU XU
Department of Electronic Engineering, Xiamen University, Xiamen 361005, China

Corresponding author: Baiqiang You (youzhou@xmu.edu.cn)

This work was supported in part by the Fujian Province Science and Technology Major Special Projects of China under Grant 2013HZ0002-1.

ABSTRACT Based on bionics, we design and analyze the left-handed (LH) characteristics of meta-elements with leaf-shaped structure. The double negative (DNG) frequency band of the initial leaf-shaped LH structure is 5.77-6.17 GHz with a fractional bandwidth of 6.7%. Inspired by two overlapping leaves, and based on topology, we evolve the leaf-shaped LH structure into a line-line coupled double-leaf LH structure. The DNG frequency bands of the line-line coupled LH structure are 2.96-3.86 GHz and 4.14-4.18 GHz. This structure not only retains some of the radiation and reflection properties of the initial design, but also gains new electromagnetic characteristics (an additional DNG frequency band). Finally, the line-line coupled LH structure is further evolved, through mostly homeomorphic deformation, into a ring-ring coupled double-veined leaf-shaped LH structure. The DNG frequency bands are 3.05-3.81 GHz and 5.31-5.41 GHz, and the fractional bandwidth are 22.2% and 1.9%, respectively. The arc-vein branches form parallel ring-ring coupling with the margin, affecting the structure's impedance and capacitance. Similar to the line-line coupling, it can locally stretch the electromagnetic characteristics, expanding the corresponding DNG bandwidth. Through the establishment of electromagnetic topological set, we classify and analyze the topological transformation and the corresponding changes in electromagnetic characteristics. We then use formula to express the process of topological transformation intuitively. Finally, the ring-ring coupled LH structure is loaded on a microstrip antenna in several different ways, improving the antenna's radiation properties, including bandwidth, directivity, and gain.

INDEX TERMS Array loading microstrip antennas, bionics, electromagnetic topological set, left-handed materials, radiation beam control, topological transformation.

I. INTRODUCTION

In recent years, many efforts have been devoted to designing novel metamaterials with left-handed (LH) electromagnetic characteristics. These LH materials (LHM) have a focusing effect on the electromagnetic wave, which can be utilized to increase the gain of antennas and improve their communication performance. Most of the designs of LHM are of conventional shapes based on the classical split-ring resonators (SRRs) model. However, regularly shaped metamaterials have some key disadvantages, such as having few adjustable parameters and limited flexibility in terms of structural design. The living organisms in nature are constantly evolving through survival of the fittest, and there are some excellent structures that are worth learning from. Therefore, it is not surprising that bionics, or biologically inspired engineering, has been applied in many fields, including antenna design. But there are still very few examples in LHM structure design.

By applying bionics principles, researchers in [1] proposed a fern inspired fractal antenna, and showed that fractal iteration can reduce the operating frequency of the antenna. In [2] a novel dual-band fractal bionic antenna resembling the branch structure of tree was designed. The antenna met the requirements of a variety of wireless applications. In [3] the Bionic Antenna Array (BAA) sensor for identifying non-contact motion was proposed. In [4] a petal-inspired deployable-foldable mechanism for space applications was proposed based on features common to the flower blooming process. In [5] a real-time stereo vision SLAM

The associate editor coordinating the review of this manuscript and approving it for publication was Raghvendra Kumar Chaudhary.

system based on bionic eyes was presented. Ref. [6] shows that reliable and comfortable advanced bionic prostheses can assist Paralympics athletes to achieve great results. In this paper, we employ bionics to design a simplified leaf-shaped LH structure and gradually evolve it through topological transformation.

Topology is concerned with certain properties that a graph keeps unchanged after continuous morphing - topological properties [7]. These inherent properties of a graphic are not affected by its shape or size. In [8] topological transformation is divided into three categories according strength: differential homeomorphic deformation, homeomorphic deformation and non-homeomorphic deformation. Among them, differential homeomorphic deformation refers to some smooth elastic deformation that maintains the current and electric field distributions, with the electromagnetic characteristics showing a continuous change. Homeomorphic deformation refers to making more obvious changes while keeping the overall structure and performance unchanged. In some cases, however, spurious frequencies may be produced. Non-homeomorphic deformation refers to tearing, combining, or gluing the structure. It has the strongest transformation intensity, and greatly affects the current and electric field distribution.

For complex LH structure, analysis based on circuit theory and electromagnetic field theory is complicated. And with large amount of calculation, the error generated by the equivalent circuit method becomes greater. In this case, circuit theory combined with topological transformation theory and set theory can be used to analyze the LH structure.

With analysis from the perspective of topology, we classify the change of the length of transmission line (TL) and the corresponding gradual change of reactance as homeomorphic transformation. If a TL is divided into two, the changes of topological structure and the electromagnetic parameters are non-homeomorphic. The mutual conversion of LHM and right-handed material (RHM) rely on discontinuity in property of the structure resulting from non-homeomorphic topological transformation, which cannot be achieved by just changing the length or size. The classic SRRs [9] can be regarded as the result of bending the two arms of a microstrip dipole. The two structures are similar in topology. But their electromagnetic properties are completely different. After the two arms are bent, a series capacitor is formed between the inner arm and the outer arm, giving the SRRs LH characteristics. Therefore, the theory of topological transformation alone is not enough for studying related structures. It is necessary to include field distribution analysis to capture the electromagnetic characteristics.

Drawing lessons from ideas related to the online database of topological electronic materials [10]–[12], based on topology and LHM electromagnetic characteristics, we begin with a few electromagnetic topology sets, and classify the changes in electromagnetic properties caused by different types of deformation. We then use formula to express the process of topological transformation intuitively.

More specifically, we design a simplified asymmetric leaf-shaped LH structure. Then the line-line coupled double-leaf LH structure and the ring-ring coupled double-veined leaf-shaped LH structure are obtained through topological transformation. The three LH structures and relevant properties are categorized as electromagnetic topology sets, and the deformation process is expressed by formula as semi-quantization. Detailed analysis revealed transformation methods that might be applicable to other microstrip antennas with relatively complex structure. In the last chapter, after comparing the LH characteristics of the three meta-elements, we choose the ring-ring coupled double-veined leaf-shaped LH structure as the basic LH unit cell for array loading. Through simulation and measurement, different arrangements of the LH unit cells are loaded on a simple microstrip antenna in several different ways, some of which are shown to improve the antenna's performance to a certain extent. At the same time, it also demonstrates the advantages of topology in guiding the design of LH structure.

II. UNIT DESIGN

A. THE ORIGIN OF THE LEAF-SHAPED STRUCTURE

Pendry *et al*. theoretically proved when thin metallic wires are periodically arranged, they have an equivalent negative dielectric constant below the plasma frequency [13]; and the periodically arranged SRRs have an equivalent negative permeability [14]. The LHM can be obtained by overlapping the negative permittivity and negative permeability frequency band. Additionally, in [8], analysis based on TL theory and experiments show that LH characteristics can arise from the combination of series capacitance (SEC) and shunt inductance (SHI). In fact, a structure similar to Fig. 3(b) has LH properties.

The natural leaf's reticulated venation shown in Fig. 3(a) is a classic example of fractal recursion. A structure with such formation may contain multiple subsystems that meet the requirements above and have the potential to achieve multiple frequency bands (some of which may overlap into one) and wide absolute bandwidth. Based on this, we designed a simplified leaf-like structure which is shown in Fig. 3(b) - a bionic design with the potential to have wide bandwidth and frequency coverage, as well as broad compatibility for antenna applications. Fig. 1 shows the origin of the leaf-shaped structure and the ground planes in each iteration in Fig. 1 are the same. Together with Fig. 2, they show each subsystem's corresponding resonance property, and hint at the multi-band potential of leaf-shaped structure with more complex vein system. An object has inherent antenna characteristics. So, from the perspective of wire antenna theory, the resonant frequency is estimated by the following equations:

$$f = \frac{c}{\lambda} \tag{1}$$

$$\lambda_g = \frac{\lambda}{\sqrt{\varepsilon_r}} \tag{2}$$

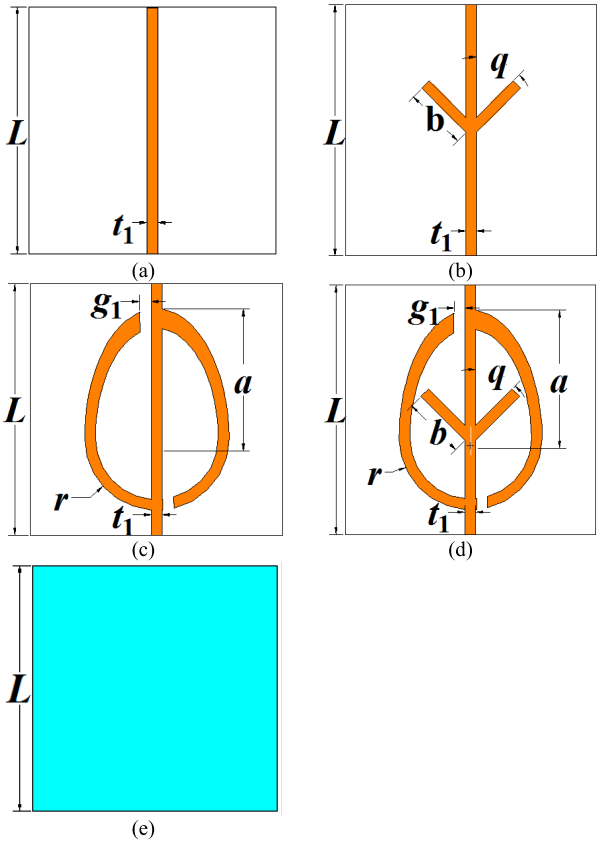

FIGURE 1. The evolution of leaf structure. The top view of (a) The main pole (midrib), (b) The midrib plus vein branches, (c) The midrib plus margin arcs, (d) The midrib plus branches and plus arcs. (e) The back view of leaf structure: ground plane.

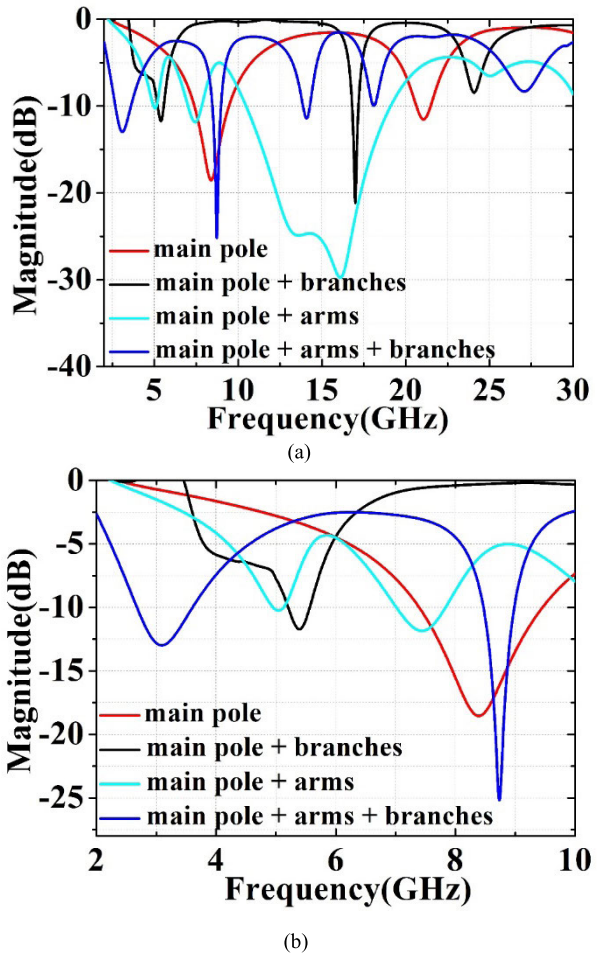

FIGURE 2. The return loss of 4 evolutionary structures. (a) 2-30GHz. (b) 2-10GHz.

where c is the speed of light ($3 \times 10\text{^}8$ m/s) and ε_r is the dielectric constant of the substrate. λ and λ_g are wavelength in free space and in the waveguide, respectively. Most of the parameters in the evolution process are retained in the final leaf-shaped structure, as shown in Table 1 (where b is 1.8 mm). The structure is loaded on FR-4 dielectric substrate with permittivity $\varepsilon_r = 4.4$, electrical conductivity tangent loss $tan\delta = 0.02$, and thickness of 1.5 mm. For Fig. 1(a). The length of the midrib is 7 mm (generally the length of the antenna is 1/4 to 1/2 wavelength), and the lowest resonance frequency is about 10 GHz. For Fig. 1(b), the branch length is 1.8 mm, and the lowest resonance frequency of the structure is about 7.5 GHz. For Fig. 1(c), the length of each arc of the ellipse margin is 6 mm, and the lowest resonance frequency of the structure is about 3.5 GHz. For Fig. 1(d), the lowest resonance frequency is about 3.3 GHz.

As shown in Fig. 2, the theoretical estimation and the simulation result are basically in agreement. The leaf-shaped structure can be regarded as a combination of leaf vein branches of different length. From Fig. 1(a) to Fig. 1(d), because current path of different length correspond to different frequency points, the resonant frequency points and bandwidth are changed when different parts are added to the midrib. Since a leaf-shaped structure can provide various combinations of current path, especially when vein branches of different length are added, the performance of such design can be further tweaked and improved with increasingly complex vein system. As a general rule, the lowest frequency points correspond to the total length of the structure whereas the highest ones correspond to the branches and sub-branches themselves. It is a fractal process that uses similarity to fill space of leaf structure by loading veins of different length. With the increase and iteration of the veins of different length, the resonant frequency of the antenna can be changed in a wide range while keeping the size of the dielectric substrate unchanged to achieve frequency reduction and width characteristics. But considering the problem of impedance matching, not every frequency point is well matched. Nevertheless, they satisfy not only sub-6G communication, but also millimeter wave and even optical frequency bands application requirements.

B. LEAF-SHAPED SINGLE FREQUENCY LH STRUCTURE

The targeted basic resonant frequency is set to 5.0 GHz. The midrib (See Fig.3(b)) in the middle and the arcs on both sides correspond to the low frequency point, and the combination

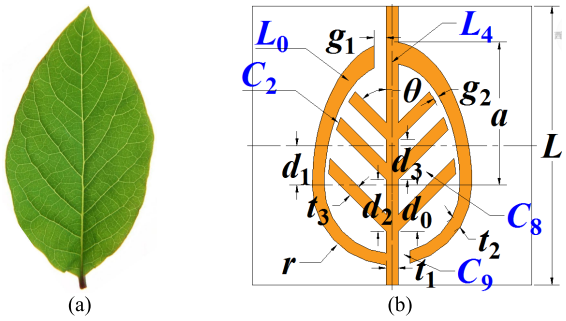

FIGURE 3. (a) Natural leaf. (b) Schema of the leaf-shaped LH structure.

of inner veins, middle stem and outer arc can generate many frequency points. Then the λ in free space and the λ_g in the waveguide can be calculated by (1) and (2). Using the 1/4 wavelength rule, considering both the medium and free space, we can estimate the total length of the middle pole should be around 7-15 mm. So, let the length of the midrib = the length of the substrate = L = 7 mm. The angle between the veins and the midrib is $\theta = 45°$.

In the leaf-shaped structure, the veins are equivalent to parallel inductors and the two openings in the margin are equivalent to series capacitors, whereas the midrib act as SHI. Additional capacitors are formed at the small gaps between the veins and the margin, which can also be seen as SEC for different current paths. There are several candidates of SEC-SHI structure within the meta-element. The vein structure including the midrib is expected to produce negative permittivity, while the two openings in the margin of the leaf and small gaps between the inner veins and the margin are expected to produce negative permeability. By adjusting the parameters of the structure, the electrical resonance and the magnetic resonance can overlap, resulting in double negative (DNG) characteristic. Table 1. lists the geometric parameters obtained through HFSS optimization. Fig. 4(a) and Fig. 4(b) shows the simulation results.

TABLE 1. Geometric parameters of the leaf-shaped LH structure (in units of mm, aside from vein-midrib angle θ).

Parameter	Value	Parameter	Value
L	7.00	a	3.80
r	2.00	d_0	1.00
d_1	1.00	d_2	1.30
d_3	1.00	t_1	0.30
t_2	0.30	t_3	0.30
g_1	0.30	g_2	0.10
θ	45°		

With traditional RHM, the phase velocity is along the direction of energy flow, resulting in a regular forward wave. This means that as the operating frequency becomes higher, the phase lag will also increase. With LHM it is the opposite and a backward wave can be observed. When the S-parameter matrix is obtained by simulation or real measurements, the expressions of refractive index and wave impedance can

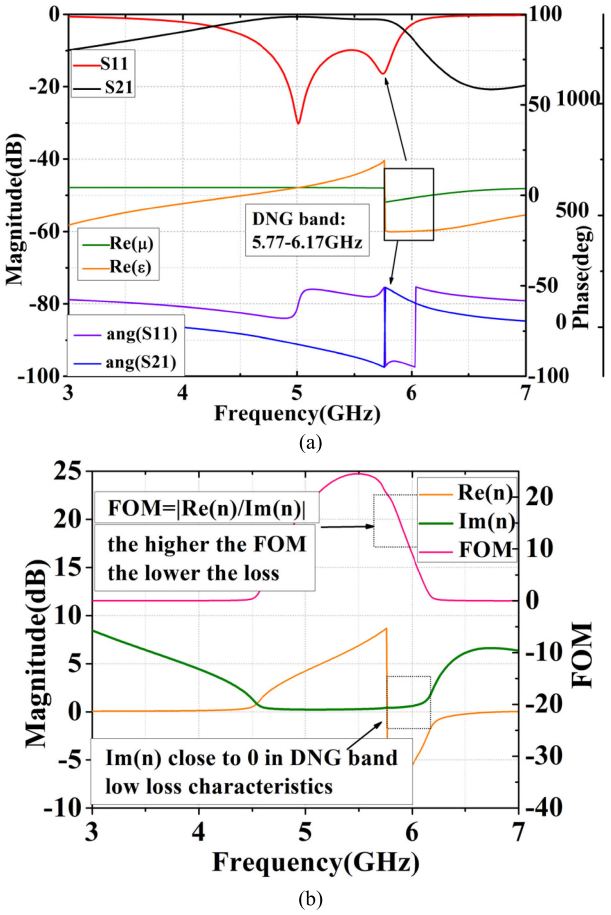

FIGURE 4. (a) Simulated S-parameters, permittivity, permeability, and phase. (b) Real *Re*(*n*) and imaginary *Im*(*n*) parts of refractive index, and figure of merit (FOM).

be inversely deduced by using S-parameter inversion method proposed in [15]. These expressions can then be used to calculate the equivalent dielectric constant and equivalent permeability. From there, the DNG frequency band of the leaf-shaped LH structure is derived as 5.77-6.17 GHz.

With the help of simulation of the surface current distribution and magnetic field distribution, we analyze which parts have notable influence on the performance of antenna in order to guide the subsequent topological transformations. As shown in Fig. 5(a), the current directions in left and right arcs of the margin are the same, forming a magnetic moment in opposition to the external magnetic field and generating magnetic resonance. Fig. 5(b) shows that, at each of the upper and lower gaps, there is a strong potential difference, which can form a strong coupling and generate plasma effect. Fig. 5(c) shows that the magnetic field is mostly confined to the left arc. The difference in magnetic field strength results in the structural imbalance that enhances magnetic resonance. As discussed above, the generation of the directional magnetic field is mainly concentrated at the elliptical margin of the leaf, so the topological transformation can be concentrated here.

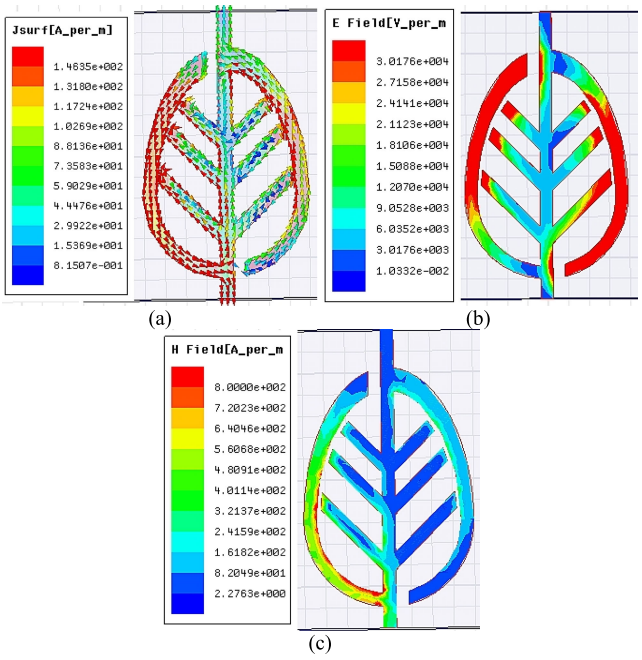

FIGURE 5. Leaf-shaped LH structure with (a) Current flow. (b) Electric field distribution. (c) Magnetic field distribution.

C. NON-HOMEOMORPHIC DEFORMATION TO LINE-LINE COUPLED DUAL FREQUENCY LH STRUCTURE

The non-homeomorphic topological transformation can change the shape of the figure greatly. It may tear, combine, or glue the figure. That is, the structure may fracture or converge at different points, or multiple figures can be combined or glued together [8]. According to TL theory, this type of transformation will significantly change the electromagnetic properties of the structure.

Inspired by the shape of two overlapping leaves (See Fig. 6(a)), we change the basic leaf-shaped LH structure to the combination of two similar units, named the line-line coupled double-leaf LH structure (See Fig. 6(b)). The vein structure is simplified, the shape of the margin is changed from ellipse to circle as the two are topologically equivalent, and the two leaves are combined in reverse. Each blade has one side of its arc shaped margin shortened and coupled with the midrib of the other blade. For the new structure in order to be able to generate negative permittivity, we keep the midribs unchanged. The inner veins of two blades form a new coupling structure, which is equivalent to a capacitor.

To make room for the subsequent topological transformation, the substrate size is changed to 10 mm. Let the diameter of the circle = the length of the midrib = 9 mm. According to the estimation based on wire antenna theory ((1) and (2)), the resonance frequency corresponding to the midrib and the arc must be lower than that of the basic leaf-shaped structure. The possible lowest resonance frequency is around 3.5 GHz. The angle between the internal branch and the midrib is changed to 25° and the length is about 5 mm. The parameters determined by simulation are listed in Table 2.

TABLE 2. Geometric parameters of the line-line coupled double-leaf LH structure (in units of mm, aside from vein-midrib angle p).

Parameter	Value	Parameter	Value
L	10.00	r	4.50
w	3.70	p	25°
d_0	2.50	d_1	1.70
t_1	0.40	t_2	0.40
g_1	0.20	g_2	0.20

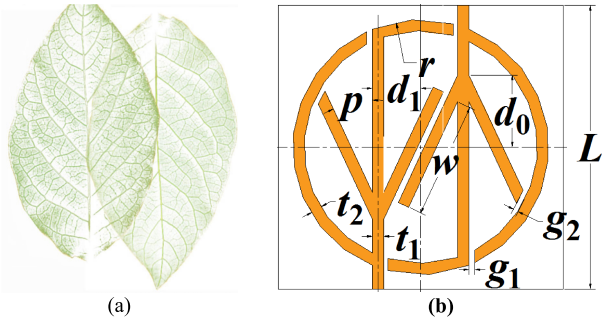

FIGURE 6. (a) Two overlapping leaves. (b) Line-line coupled double-leaf LH structure.

The simulation results are shown in Fig. 7(a). Compared with the original leaf-shaped LH structure, the line-line coupled double-leaf LH structure produces two DNG frequency bands, which are 2.96-3.86 GHz and 4.14-4.18 GHz (adding one wide low-frequency DNG band). From the perspective of equivalent-circuit theory, the overall circuit of this structure is composed of two identical circuits of the deformed leaf-shaped LH structure, plus three capacitor connections formed between them. Moreover, based on their sizes, we can estimate the current paths going through the two midribs correspond to low frequency, and those oscillate in the veins correspond to high frequency. The new line-line parallel coupling of the two inner veins may offer possible explanation as to why the new structure is able to produce wide negative permittivity bands even though the vein structure of each blade is simplified.

From the perspective of topological transformation, the double-leaf LH structure is a short-range interaction of two identical LH units that are derived from the original leaf-shaped LH structure through homeomorphic deformation. The short-range interaction is an essential change that is non-homeomorphic, which will greatly affect the electromagnetic properties of the structure. While with homeomorphic deformation the new structure is expected to inherit the properties of the original. Therefore, when the two are performed together, new electromagnetic characteristics may be generated on the basis of maintaining some of the electromagnetic properties of the original structure. That is, an extra frequency band with LH characteristic is realized by adjusting the capacitance and inductance. Therefore, non-homeomorphic topological deformation may lead to a change in the performance of the unit structure at certain frequencies from RHM to LHM, which is an important turning point in terms of electromagnetic properties.

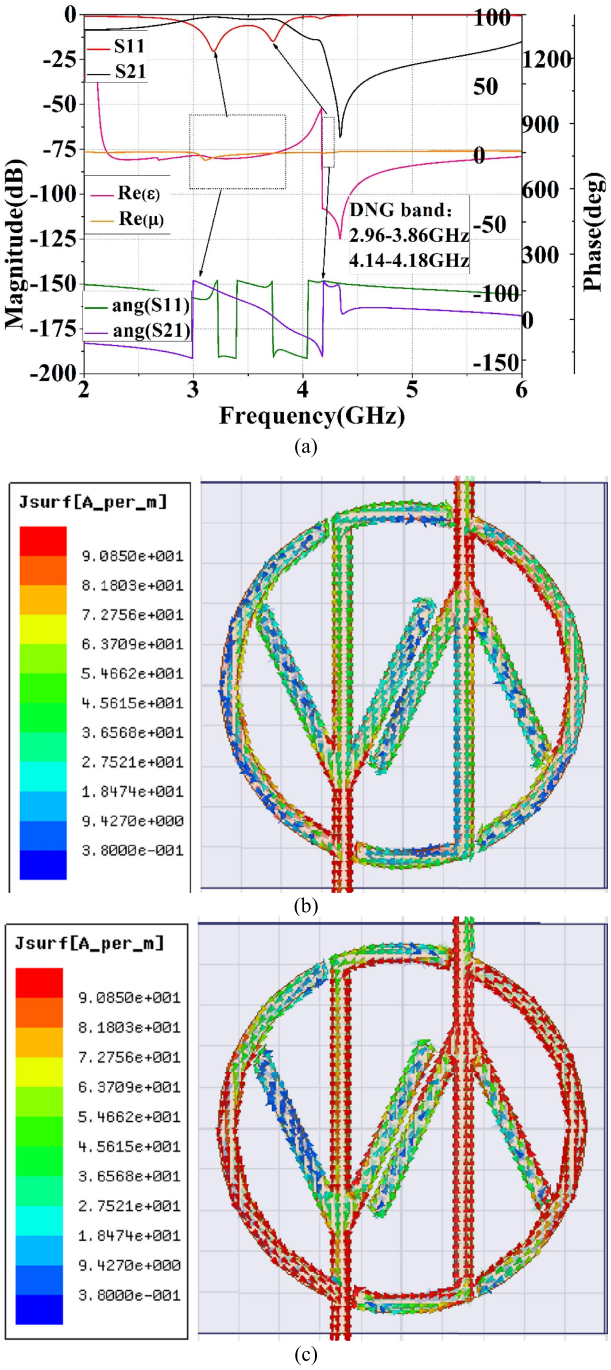

FIGURE 7. (a) S-parameters, permittivity, permeability, and phase. Current distribution at (b) 3.10 GHz. (c) 4.14 GHz.

The current distribution of the line-line coupled double-leaf LH structure at 3.10 GHz and 4.14 GHz can be used to further explain the generation of the two DNG frequency bands. At 3.10 GHz, as shown in Fib. 7(b), a co-current is formed at the right side of the structure, going through the right long-arc and the right midrib. It can produce a magnetic moment in the presence of the applied magnetic field and generate magnetic response. When the magnetic resonance strength is greater than the applied magnetic field strength, negative equivalent

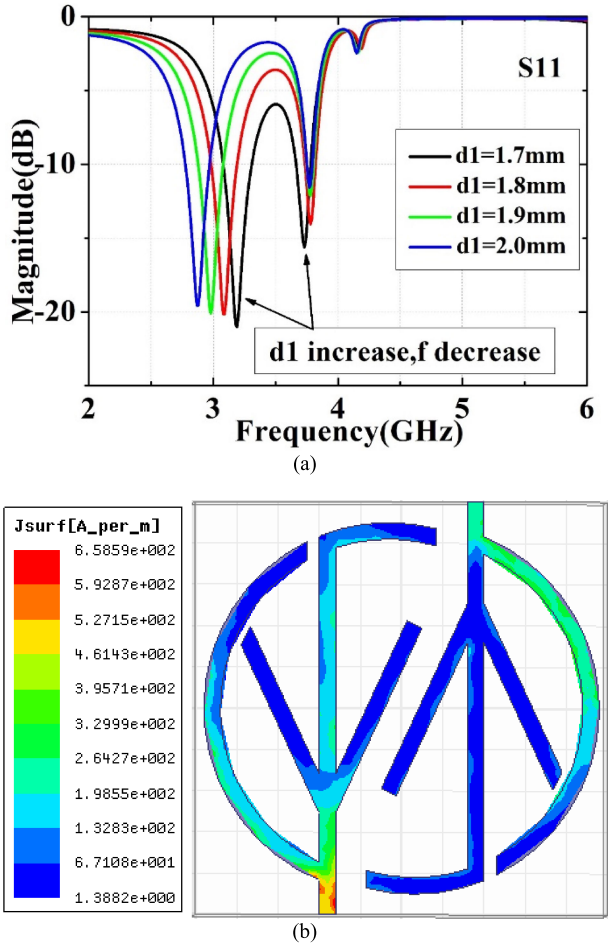

FIGURE 8. (a) The influence of d_1 on resonance frequency. (b) Current distribution with $d_1 = 2.0$ mm.

permeability is obtained. Similarly, Fig. 7(c) shows the formation of a reverse magnetic moment at the region enclosed by the left midrib, the two short-arcs, and the right midrib, at 4.14 GHz.

The effect of the parameter d_1 on the resonance frequency of the line-line coupled structure is shown in Fig. 8(a). The low frequency point decreases with the increase of d_1, whereas the high frequency point slightly increases with it. The current distribution of the line-line coupled structure is mainly concentrated in the midribs and the circular margin. This is unchanged between Fig. 7(b) and Fig. 8(b). So, changes to d_1 has a greater impact on the low-frequency point. And since the current intensity and distribution in the internal veins remain mostly unchanged, the high-frequency point is hardly affected.

D. HOMEOMORPHIC DEFORMATION TO RING-RING COUPLED DUAL FREQUENCY LH STRUCTURE

Homomorphic deformation is a certain type of topological transformation whose deformation strength is weaker than that of non-homeomorphic deformation [8]. When such transformation is applied to an LH structure, the resulting

meta-element inherits the prototype structure's characteristics and may obtain new features. This provides an idea for improving the performance of an existing LH structure.

Inspired by reticulated venation of leaves in nature (See Fig. 9(a)), the left and right outer veins of the line-line coupled double-leaf LH structure branch sideways along the margin into arc-veins, forming the ring-ring coupled double-veined leaf-shaped LH structure shown in Fig. 9(b). Compared with the line-line coupled structure, the midribs and outer arcs remain unchanged, so the corresponding low-frequency point remains the same according to estimation based on wire antenna theory. The inner arc length (going across the connection point) is about 7 mm and the high frequency point is about 5.3 GHz.

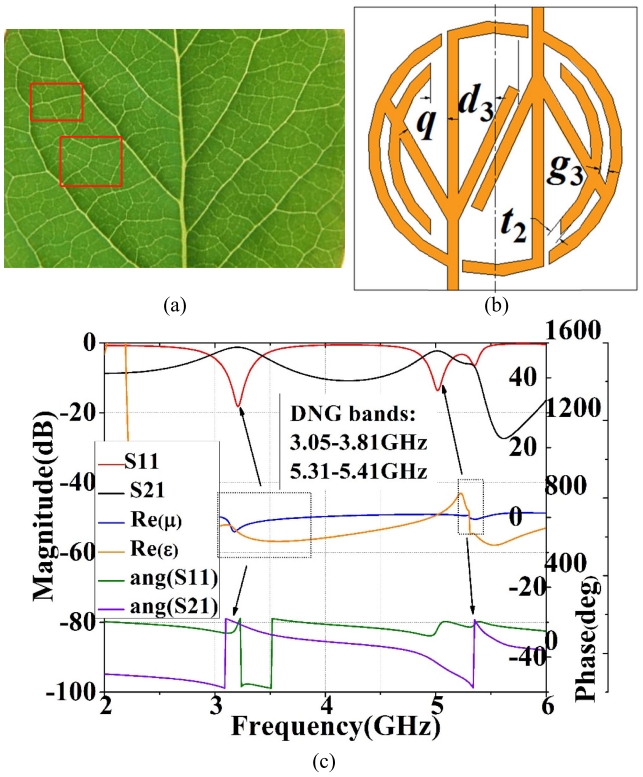

FIGURE 9. (a) Reticulated venation of natural leaf. (b) The ring-ring coupled double-veined leaf-shaped LH structure. (c) S-parameters, permittivity, permeability, and phase.

In the ring-ring coupled LH structure, the rotation angle of the four straight veins is changed to $q = 30°$. Other geometric parameters remain the same as those shown in Fig. 6(b) and Table 2, whereas new ones are labeled in Fig. 9(b) and listed in Table 3. Fig. 9(c) shows the simulated parameters. The new meta-element's DNG frequency bands are 3.05-3.81 GHz and 5.31-5.41 GHz, and the fractional bandwidth are 22.2% and 1.9%, respectively. The addition of the arc-veins moves the high resonant frequency point forward, while simultaneously expanding the high-frequency DNG band.

This is because branching increases the electrical length of the structure. When the effective path of current is increased and new couplings are formed, the equivalent inductance and capacitance of the structure are changed, causing the resonance frequency to increase. And similar to previous analysis, modification to current paths going through the vein structure corresponds to changes in the meta-element's high-frequency characteristics. Furthermore, as parallel coupling results in variable current path based on where the jump off point is from one side of the equivalent capacitor to the other, the high-frequency DNG band is expanded.

TABLE 3. Geometric parameters of the ring-ring coupled double-veined leaf-shaped structure (in units of mm, aside from angle q).

Parameter	Value	Parameter	Value
d_3	2.30	t_2	0.40
g_3	0.30	q	30°

From the perspective of topological transformation, adding the arc-veins and extending them are both topological extensions belonging to homeomorphic deformation, while connecting the inner branches with the outer ring belongs to non-homeomorphic deformation. The ring-ring parallel coupling between the arc-veins and the margin resembles the line-line coupling first introduced in the previous structure. Moreover, since the size of the arc-veins is small, their effects on current paths mostly corresponds to high frequency. Therefore, the branching should have a greater impact on high-frequency characteristics. In a word, the change in the topological properties of the graph leads to the change in the electromagnetic parameters of the structure. Homeomorphic transformation and non-homeomorphic transformation can adjust performance on the basis of retaining part or most of the original characteristics, which is useful for improving LHMs.

The bionic leaf-shaped LH structure has the advantage of DNG bandwidth expansion through sideways branching of the veins near the margin, or more specifically, the type that extends along the margin and form parallel coupling with it. Compared with the single-frequency LH structure in [16], the meta-element with dual-frequency characteristics can provide the basis for subsequent implementation to improve microstrip antennas for dual-frequency coverage. And compared with common LH structures such as those in [17]–[19], the proposed design has the following advantages: small size, single-sided, multiple adjustable parameters, easier to produce, easier to integrate into application, and complex venation of natural leaf as template to explore further improvements. For microstrip antennas with topologically similar structures, such as the UWB antennas in [20] and [21], it could be possible for researchers and engineers to apply similar transformation methods to increase the bandwidth at different frequency ranges, which is worthy of further study.

Fig. 10(a) shows as vein-midrib angle q increases, the effective current path increases (lower resonant frequency points). When effective current path becomes longer, the average magnetic flux generated by the structure in

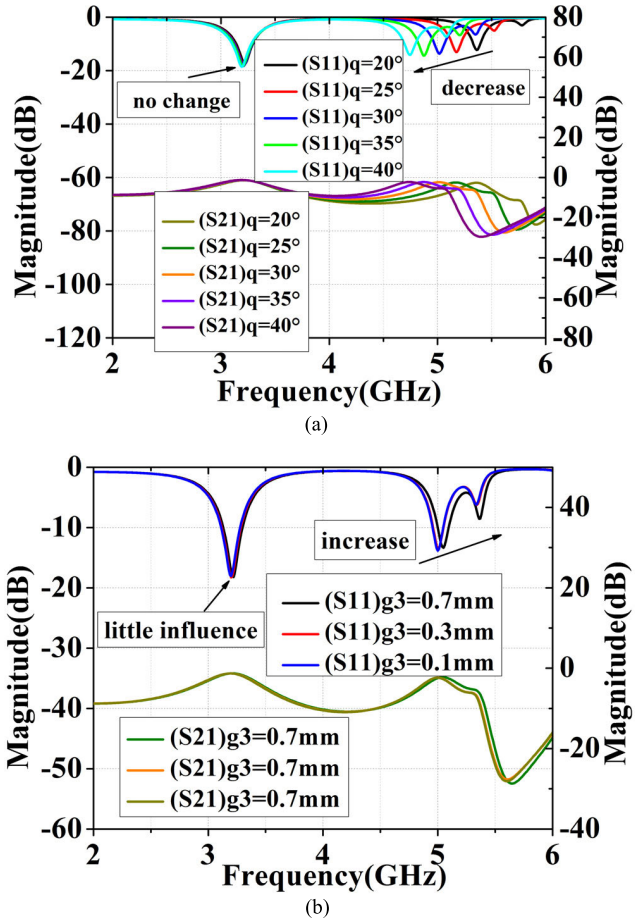

FIGURE 10. Simulated S_{11} and S_{21} for different parameters. (a) q. (b) g_3.

the electromagnetic field increases, and the overall magnon intensity change. As a result, the frequency of magnetic resonance decreases, and the corresponding DNG frequency band move to the left. Fig. 10(b) shows increasing gap width g_3 of the ring-ring coupling will reduce not only the equivalent capacitance of the circuit, but also the average magnetic flux of the overall structure. Therefore, the magnetic resonance frequency of the structure increases. In conclusion, we can adjust the high-frequency DNG band by adjusting the relevant geometric parameters according to application needs.

III. ANALYSIS OF LEAF-SHAPED LH STRUCTURES BASED ON ELECTROMAGNETIC TOPOLOGY SETS

If structures of all leaves in nature are established as a set, then the three LH structures designed in this paper are subsets of the natural leaf set, namely the leaf-shaped set (A), the double-leaf non-homeomorphic combination topology set (B) and the homeomorphic vein extension topology set (C). Based on geometric topology and LHM electromagnetic theory, different topological transformations and the changes in electromagnetic properties caused by them are classified through the establishment of sets. Then, formulas can be used to semi-quantify the process of the deformation, making it more intuitive. The leaf-shaped set is the prototype of the latter two sets and it serves as a comparison here, so only the latter two are analyzed in detail.

The elements in the leaf electromagnetic topology set include the topology, electromagnetic, and radiation characteristics of the structure. The double-leaf combined line-line coupled LH structure is composed of two identical leaf structures, each obtained through homeomorphic deformation on the original leaf-shaped LH structure. Here, the original leaf-shaped LH structure belongs to A, *and* the set of slightly deformed leaf-shaped LH structure is defined as A, whereas $\oplus$ is defined as the short-range interactive combination of two slightly deformed leaves. Then the line-line coupled double-leaf LH structure can be represented by the following formula:

$$B = A' \oplus A' \tag{3}$$

From the analysis based on topology, the short-range interactive combination of two identical geometric figures is an essential change in the topological structure. In terms of radiation characteristics, the combination of the two identical blades produces a new coupling effect, adds new inductance (midrib) and capacitance (coupling between structures). On the other hand, the preceding changes from A to A removed several short inductors (veins) along with their capacitor connection (vein-margin). Overall, when compared with A, the resonance frequency of B is reduced as seen in Table 4. In terms of electromagnetic characteristics, the equivalent circuit of the two blades is connected by the line-line coupling capacitor and the gap capacitors between midribs and the shortened arc-margins. The equivalent circuit of the entire structure has changed, and a DNG frequency band is newly added. Estimated from their size, the current paths going through the two midribs correspond to low frequency, and those oscillate in the veins correspond to high frequency.

The vein extension ring-ring coupled LH structure is obtained by extending the outer veins sideways on the basis of the double-leaf combined line-line coupled LH structure. Here, symbol $\approx$ represent the sideways extension of veins along the margin, and $+$ is defined as the combination of the double-leaf line-line coupled LH structure and the extended arc-veins. The ring-ring coupled doubled-veined leaf-shaped LH structure can then be expressed by formula as follows:

$$C = B+ \approx \tag{4}$$

From the perspective of topology, there are no essential changes made to the structure when the veins are extended sideways. So, the overall LH characteristics will mostly remain the same. In terms of radiation characteristics, the equivalent electrical length of the structure increases because of the arc-vein extensions. Thus, the current path increases. Since the topological transformation only occurs in the veins, it has little effect on low-frequency properties, but has a significant effect on high-frequency performance. When the effective path of current is increased and new

coupling is formed, the equivalent inductance and capacitance of the structure are changed, causing the high-frequency resonant point to increase. In terms of electromagnetic characteristics, the number of DNG frequency bands has not changed, and the new arc-veins form parallel coupling with the margin, increasing the bandwidth of the high-frequency DNG band.

The above analysis based on bionics, topology, and electromagnetism can be summarized as follows:

The short-range interactive combination of two identical deformed leaf-shaped LH structure through coupling connections, including the unique parallel line-line coupling, significantly changes the equivalent circuit. The resulting new current paths that correspond to low frequency lead to the formation of a new wide DNG band, achieving the purpose of expanding the absolute bandwidth.

Sideways branching near the end of the small veins along the margin can locally stretch the electromagnetic characteristics (wider high-frequency DNG bandwidth, higher resonance frequency) through the formation of parallel ring-ring coupling between the arc-veins and the margin. We can guess that as the arc-veins continue to extend along the margin, or when more subordinate veins with coupling connections to the margin are created through branching, the corresponding high-frequency DNG band will move forward and expand. Regarding the second proposition, the possible effects of additional subordinate veins coupled with the margin is also indicated by the higher position and wider bandwidth of high-frequency DNG band of the initial leaf-shaped LH structure (See Table 4.). It has multiple parallel veins with capacitor connections to the margin, and the veins can be seen as small branches arising from the midrib.

TABLE 4. Frequency characteristics of the three LH structures.

Frequency characteristics	Leaf-shaped LH structure	Line-line coupled LH structure	Ring-ring coupled LH structure
Resonance frequency (GHz)	5.00 5.77	3.19 3.73	3.21 5.02
Negative permittivity (GHz)	5.77-7.00	2.25-3.71 4.14-6.00	2.31-4.95 5.31-6.00
Negative permeability (GHz)	5.77-6.17	2.96-3.86 4.14-4.18	3.05-3.81 5.31-5.41
DNG band (GHz)	5.77-6.17	2.96-3.86 4.14-4.18	3.05-3.81 5.31-5.41

Moreover, the resonance frequency can be modified by changing the geometric parameters of different parts of the structure, which leads to changes in equivalent inductance and capacitance. And the corresponding DNG band may cover RF, millimeter wave, and even optical bands.

The design and modification process of the three leaf-shaped LH meta-elements demonstrated that with the help of bionics and topology, it is possible to obtain and tweak desirable LH characteristics through qualitative analysis of the structure, mitigating some of the complexities of circuit theory and electromagnetic field theory.

IV. PRACTICAL APPLICATION FOR ANTENNAS

A. BASIC MICROSTRIP ANTENNA

A microstrip antenna fed by coaxial line (See Fig. 11) working at 5G low frequency (3.40-3.60 GHz) is loaded on FR-4 dielectric substrate with permittivity $\varepsilon_r = 4.4$, electrical conductivity tangent loss $tan\delta = 0.02$, and thickness of 1.6 mm. The size of the substrate for microstrip antenna is usually twice the size of the patch, so the width of the radiation patch is about half of the substrate's width, and adjustments are also made to leave room for periodic loading of LH structure unit cells. According to theoretical estimation, the final geometric parameters determined by simulation are shown in Table 5. The distance between the feeding position and the y-axis is $d_0 = 3.3 \times k$, and its distance from the x-axis is $d_1 = 5.1 \times k$. Through optimization, as shown in Fig. 13 (a), when both frequency points have good resonance, the value of k is 0.8.

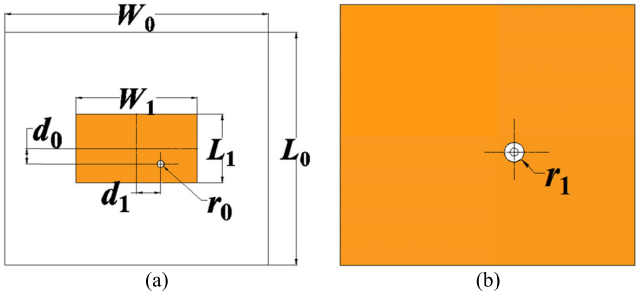

FIGURE 11. The basic microstrip antenna. (a) Front side. (b) Back side.

TABLE 5. Geometric parameters of microstrip antenna (in units of mm).

Parameter	Value	Parameter	Value
L_0	40.00	W_0	45.00
L_1	11.80	W_1	20.70
d_0	2.64	d_1	4.08
r_0	0.60	r_1	1.50

The generation of dual frequency can be verified by the electric field distribution of the microstrip antenna as shown in Fig. 12. The electric field distribution is similar, but can achieve dual frequency points in order to coincide with the resonance frequency of the ring-ring coupled LH unit.

It is found through simulation that the size of the dielectric substrate has very little effect on the resonance frequency of the antenna (See Fig. 13(b)). As shown in Fig. 13(c), we analyzed the influence of the length and width of the radiation patch on the return loss of the antenna. When W_1 is increased, the frequency of the second resonant point barely changes whereas its resonance intensity decreases. Meanwhile the first resonant point shifts towards low frequency with increased resonance intensity. On the other hand, the effect of L_1 on the antenna is the opposite. The frequency of the first resonant point is not changed by much with the increase of L_1, and its resonance intensity is increased.

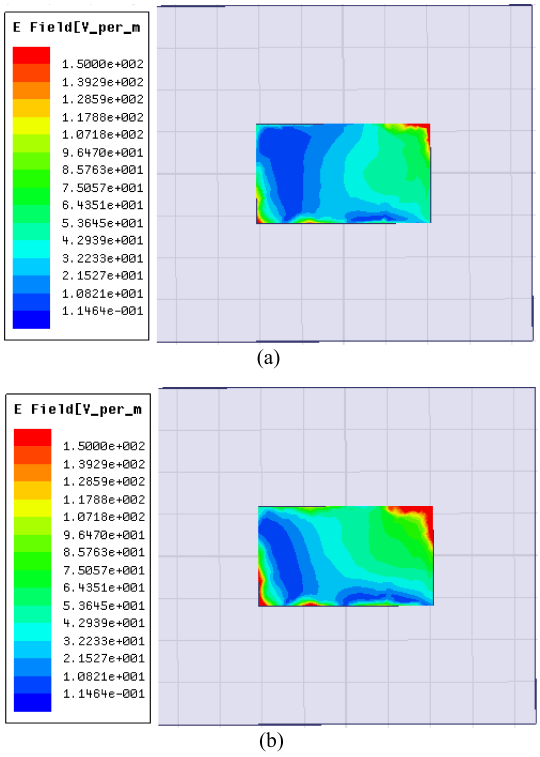

FIGURE 12. Distribution of microstrip antenna surface current at (a) 3.38GHz. (b) 5.41GHz.

Whereas the second resonant point shifts towards lower frequency and has slightly less resonance intensity with the increase of L_1. The diagonal power feed generates two resonance frequency points. Changing L_1 and W_1 only affects the corresponding frequency point.

B. AROUND MICROSTRIP ANTENNA

Due to the existence of surface waves, a basic microstrip antenna usually has the following disadvantages: low working efficiency, reduced gain, and poor directivity. The mutual interference between antenna elements can form parasitic radiations. However, with LHM the direction of wave vector is opposite to the energy direction, which makes the evanescent wave into an enhanced field. It can strengthen the antenna's signal radiation and reception, and improve the antenna's gain. In addition, the addition of LHM to the substrate results in negative refraction of the surface wave at the material's boundary, forming a closed loop. Therefore, the edge radiation of the antenna can be suppressed, the interference between the antenna elements can be reduced, and the directivity of the antenna can be improved.

In this paper, the single-sided ring-ring coupled double-veined leaf-shaped LH structure is periodically arranged on the substrate around the antenna patch (See Fig. 14). and are expected to improve the performance of antenna [22]. Table 6. lists the parameters of the LH unit cell array.

The boundary condition of a typical LH unit structure simulation is equivalent to an infinite plane filled with

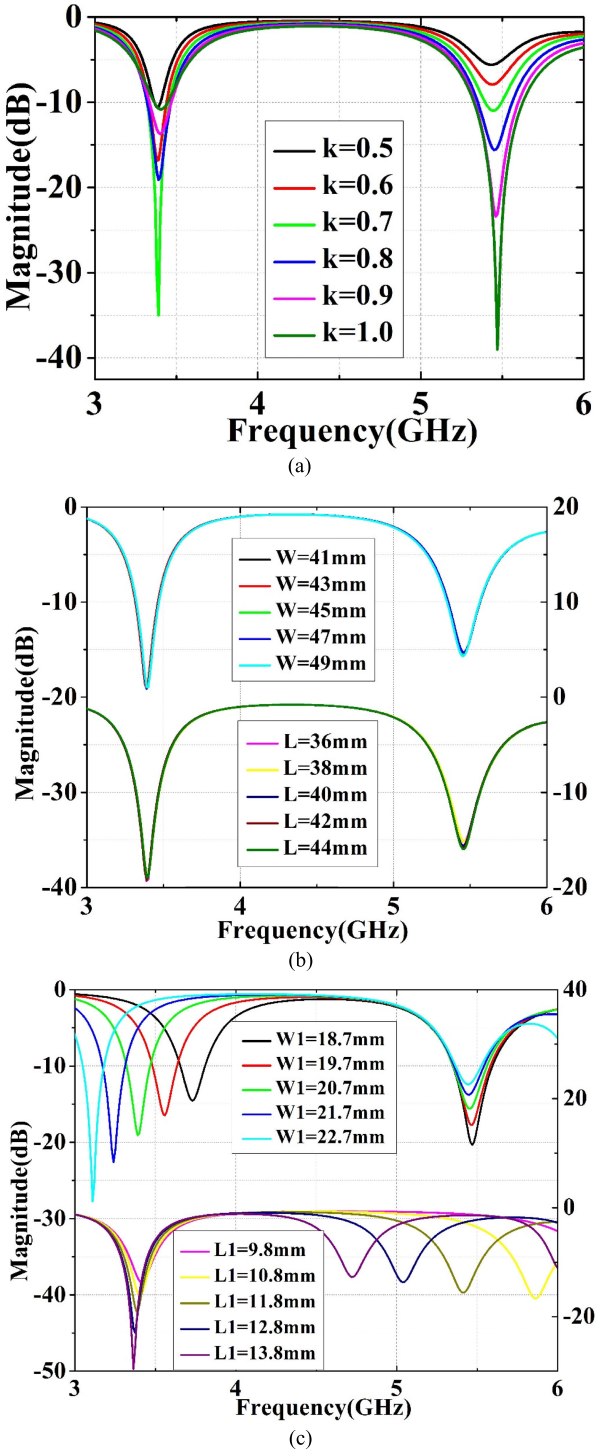

FIGURE 13. Influence of structural parameters on resonant frequency points of the basic microstrip antenna (a) Feed position. (b) Length and width of substrate. (c) Length and width of radiation patch.

uniformed array of the LH unit cells in the same direction. When a limited number of LH unit cells are used in a loading arrangement, each unit's performance will deviate from that of the isolated LH unit structure simulation.

Fig. 15 shows the electric field distribution of the peripheral array loading and the array rotation loading of LH unit

TABLE 6. Parameters of the loading arrangement (in units of mm).

Parameter	Value	Parameter	Value
d_x	13.00	d_y	10.50
g_x	7.00	g_y	6.50

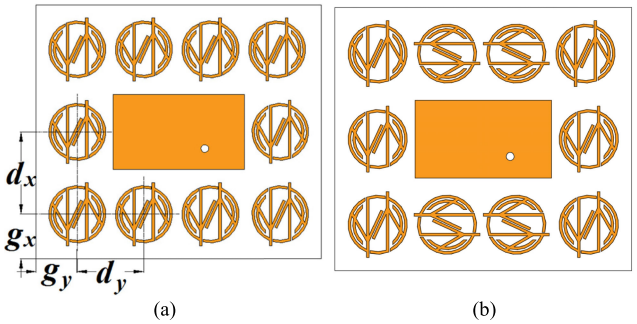

FIGURE 14. The structure of microstrip antenna with (a) Array loading, (b) Array (rotation) loading.

cells. Compared with the basic microstrip antenna, the electric field is no longer only distributed at the two corners.

Fig. 16(a) and 16(b) shows that the lobe width is reduced at 1st and 2nd resonant frequency points, indicating enhanced directivity. Fig. 16(c) shows the S_{11} in three loading cases. Loading the ring-ring coupled LH structure increases the bandwidth of the microstrip antenna. When some of the LH unit cells are rotated, the electric field increases at the second frequency point (Fig 15(d)), and the gain here decreases.

Although both loading methods improve the antenna performance, array loading without rotation yields better results. This is caused by the increased inconsistency between the rotated LH unit cell arrangement and the boundary conditions of the LH unit structure simulation.

In addition, we analyze the influence of the loading position of the ring-ring coupled LH structures on the S-parameters. Symbol x represents how much each of the two columns of LH unit cells moves horizontally towards the microstrip antenna, whereas n represents the vertical distance between center points of adjacent LH structures from different rows ($x = 0$, $n = 13$ mm is the original arrangement from Fig. 14). It can be seen from Fig. 17(a) that as the lateral distance between the columns of LH unit cells and the microstrip antenna decreases, the resonance strength of the low-frequency resonant point is increased, and it's position also slightly shifts to the left. But the adjustments have little effect on the high-frequency resonant point. It can be seen from Fig. 17(b) that as the vertical distance decreases, the resonance strength of the low-frequency point is enhanced. Considering the aberrations at high-frequency resonant point shown in Fig. 17(b), $n = 13$ mm is selected to achieve good performance at both frequency points.

Finally, the physical prototype of microstrip antenna with array loading is shown in Fig. 18(a) and 18(b). And the

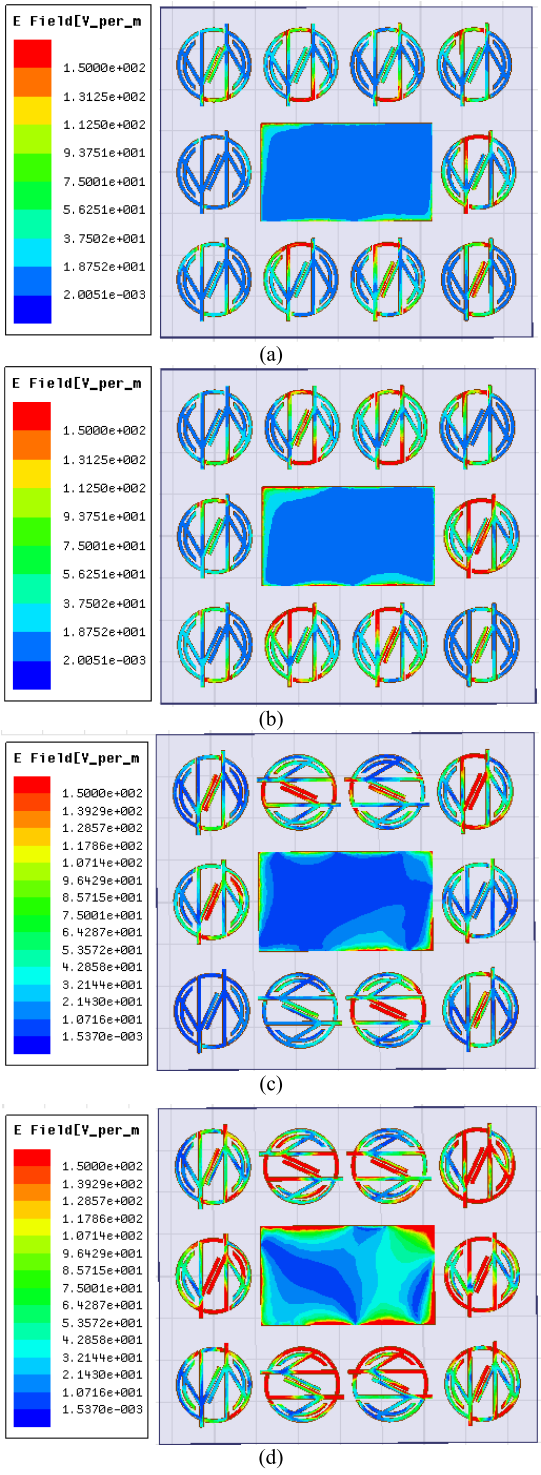

FIGURE 15. The electric field distribution after loading the LH structure. (a) With array loading at 3.38 GHz, (b) With array loading at 5.5 GHz. (c) With array rotation loading at 3.38 GHz, (d) With array rotation loading at 5.5 GHz.

simulation results are mostly in agreement with the measured results (See Fig. 18(c)). The slight change of S_{11} is mainly due to the deviation in the gap width when the antenna is fabricated and the influence of environmental factors during the measurement.

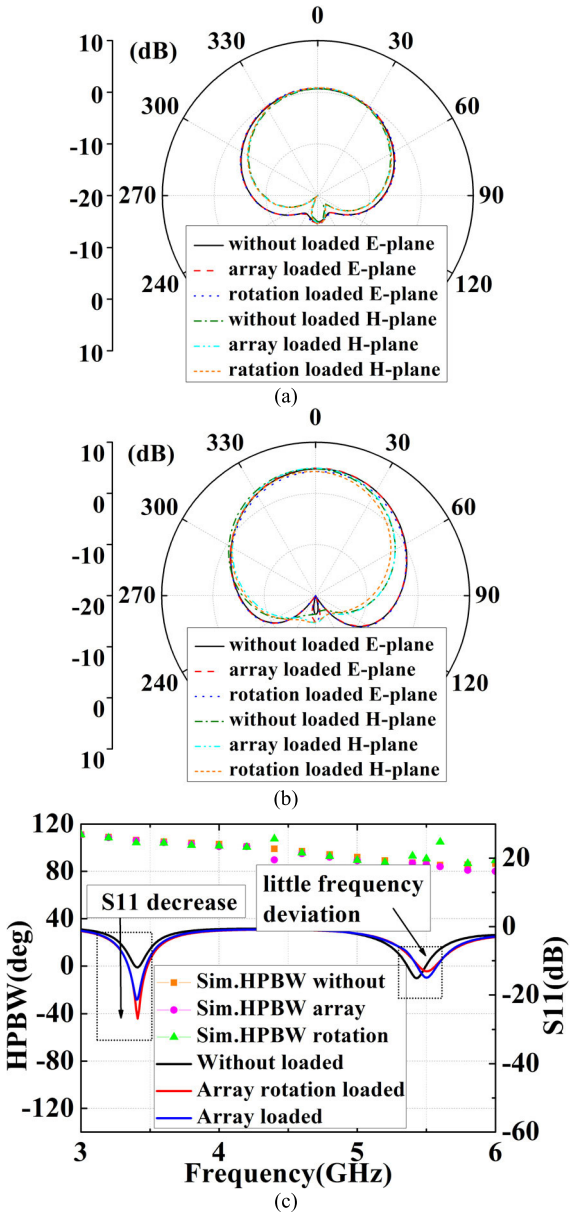

FIGURE 16. Simulated radiation patterns in three loading cases. (a) 3.38 GHz. (b) 5.5 GHz. (c) Simulated S_{11} and half-power beam width (HPBW) at E-plane.

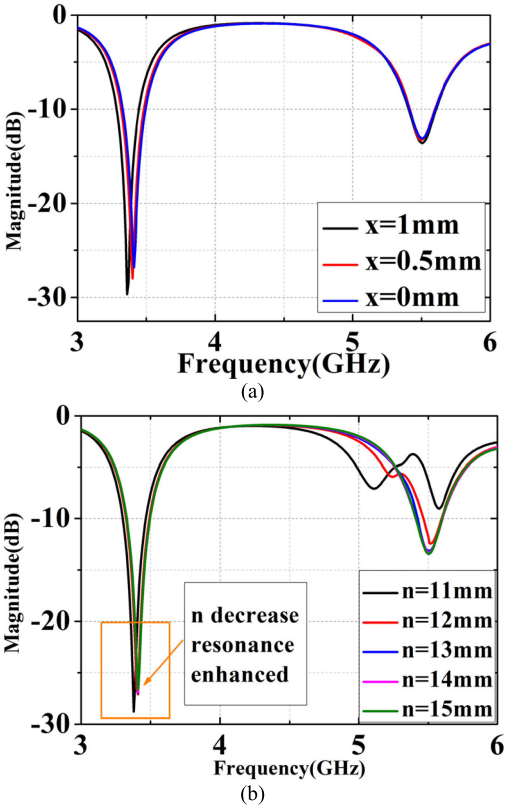

FIGURE 17. The influence of LH unit cells' position on S-parameter S_{11} in terms of (a) Horizontal shift x. (b) Vertical spacing n.

C. COVERED MICROSTRIP ANTENNA

LHM are known to have negative refraction properties [23], [24]. And using them as antenna cover layers can cause the electromagnetic waves to converge, enhancing the directivity of the antenna and increasing its gain. So, a double-veined leaf-shaped LH structure array containing 3 × 3 unit cells are used as overlay, which is placed on top of the microstrip antenna with distance h (See Fig. 19(a)). The horizontal spacing (between edges) of LH unit cells is changed to 7.5 mm. Fig. 19(b) shows the simulated S-parameter S_{11} when h is set to $\lambda/6$, $\lambda/4$, $\lambda/2$, λ, 2λ (wavelength $\lambda = 56$ mm).

When h is smaller than λ, both resonance points slightly shift to higher frequency, and when h is greater than λ, the two points shift towards low frequency. When h is $\lambda/4$, the return loss is the lowest. Compared with the microstrip antenna without loaded LH unit cells in Fig. 16(c), the covered model with $h = 14$ mm has significantly improved directivity and greatly increased gain at both resonance frequencies (by 3.44 dB and 1.63 dB). The forward and backward radiation are both enhanced after adding the cover layer. When h is $\lambda/4$, the impedance matching of the antenna at the high-frequency resonant point is the best. And when h is between $\lambda/4$ and $\lambda/2$, a superposition of electromagnetic oscillations is formed, resulting in the strongest resonance.

In addition, when cover layer is added, the H-plane pattern resembles the shape of a one-sided figure-8, indicating that energy is concentrated in the normal direction of the radiation patch. Therefore, loading the cover layer can control the radiant energy of the antenna to gather in the normal direction and improve the normal gain. Fig. 20 shows the radiation pattern when h takes different values. The unloaded microstrip antenna has the smallest backward radiation. After loading the array overlay, when h is smaller than λ, the backward radiation is greater, indicating better directivity; when h is bigger than λ, the side lobes of the antenna gradually increase, reflecting omnidirectional properties. According to the above analysis, it can be known that when the distance is between $\lambda/4$ and λ, the performance of the antenna will be improved to the greatest extent.

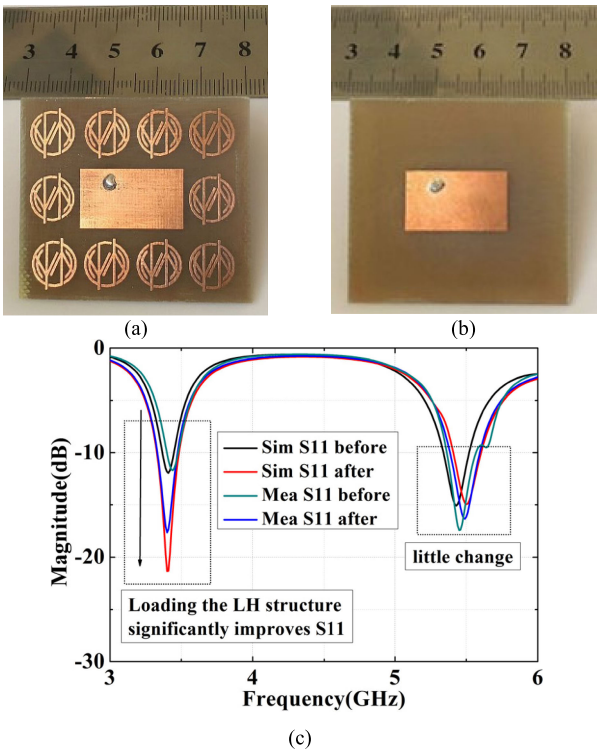

FIGURE 18. Prototype of the microstrip antenna (a) With array loading, (b) Without loading. (c) Simulated and measured S_{11}.

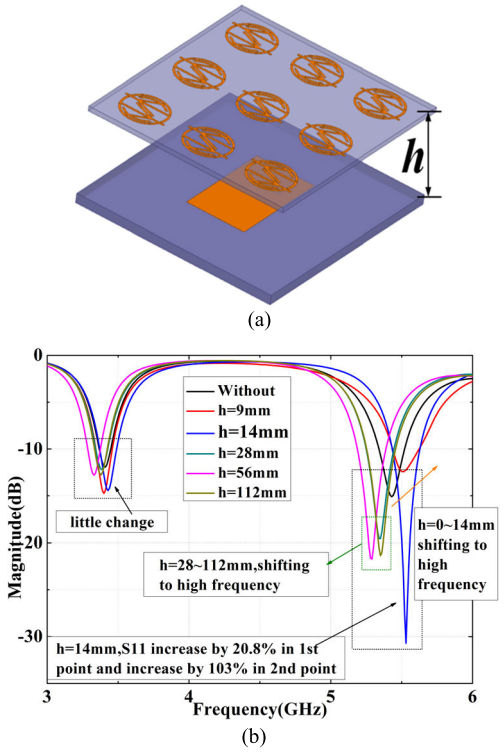

FIGURE 19. (a) 3 × 3 array overlay. (b) Simulated S_{11} for different h.

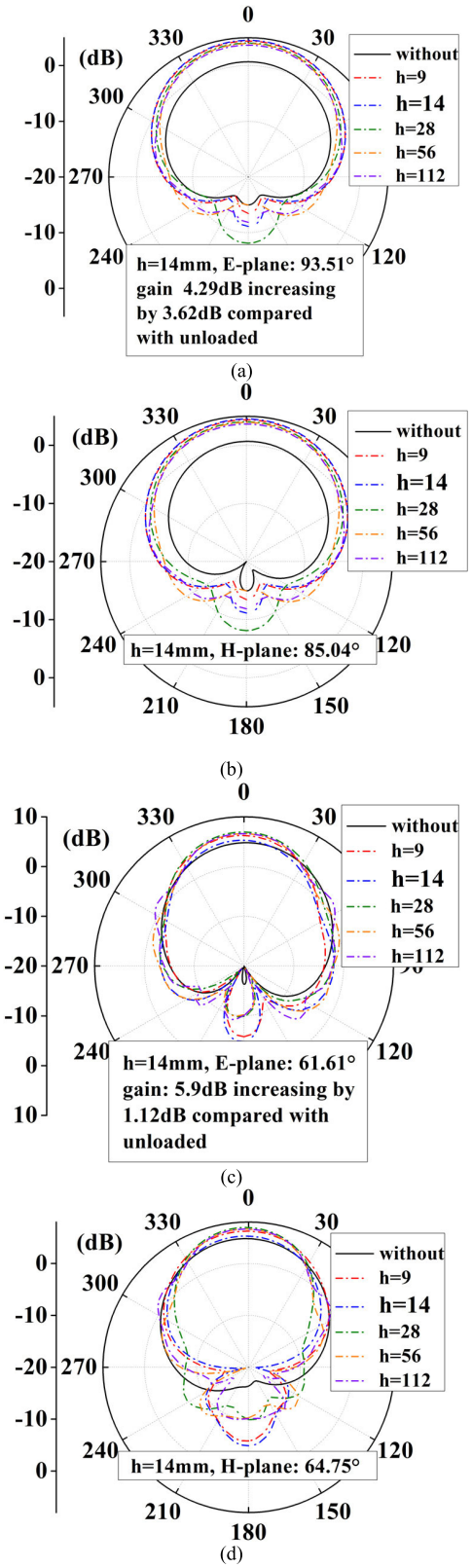

FIGURE 20. Simulated radiation pattern for h. (a) 3.43 GHz E-plane. (b) 3.43 GHz H-plane. (c) 5.5 GHz E-plane. (d) 5.5 GHz H-plane.

D. TWO OVERLAYS COVERED MICROSTRIP ANTENNA

Next, the 3 × 3 overlay is split into two overlays then stacked on top of the microstrip antenna as seen in Fig. 21(a). In order to reduce the coupling effect between the LH unit cells, the first layer is set as four LH unit cells and the second

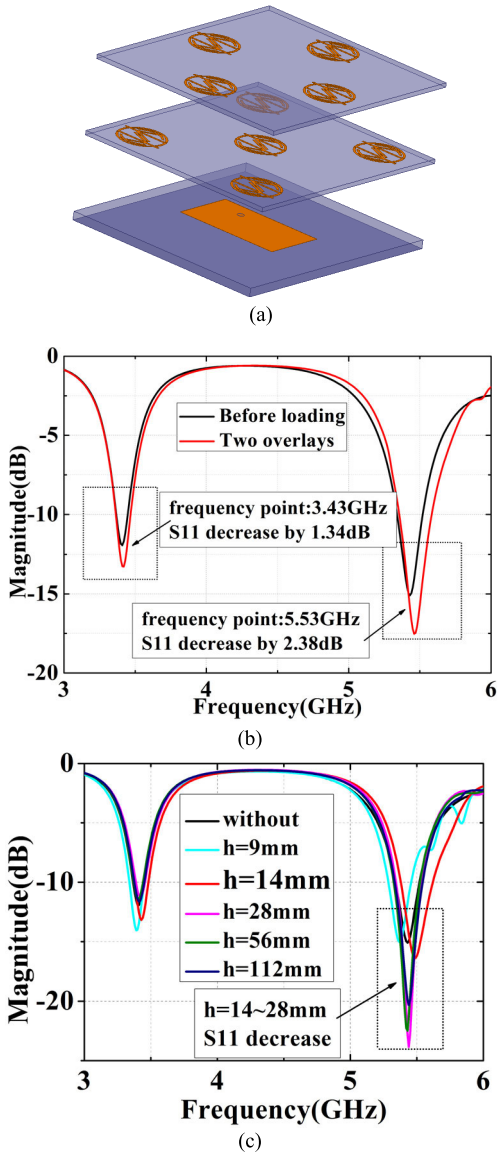

FIGURE 21. (a) The model of two overlays. (b) Simulated S_{11} with two overlays. (c) The influence of different h on S_{11}.

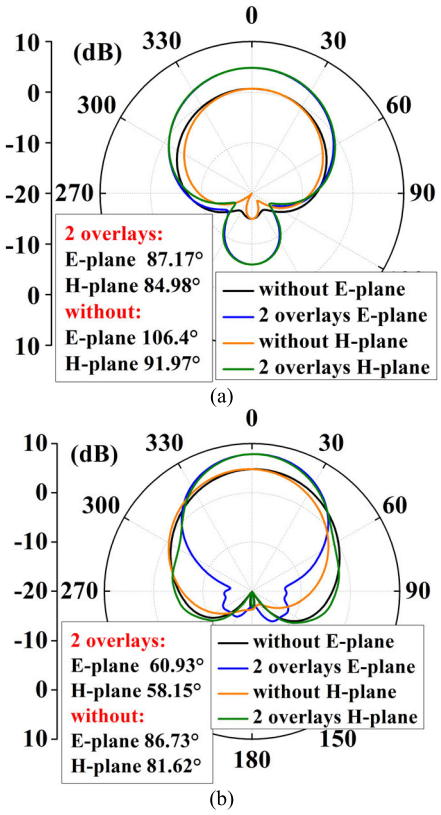

FIGURE 22. Simulated radiation patterns with two overlays when h = 14 mm and unloaded. (a) 3.43 GHz. (b) 5.5 GHz.

TABLE 7. Compared with previous research works.

Ref	Bandwidth	Gain(dBi)	HPBW	Efficiency
AWP.2019.290183828	48%	9.2±0.5	58.5°±4°	~82%
TBCAS.2020.3010259	11.5%	2.1	/	~87%
LAWP.2020.2979492	/	7.21±0.36	/	~87%
LAWP.2008.2011656	65.9%	9.5	61°±3°	/
TAP.2012.2214998	68%	6.6~9.6	~56°	~65%
TAP.2019.2927646	9%/5%	6.0	154°	90%
Prop	**3.3%/4.2%**	**7.84**	**58.15°**	**~83.4%**

layer as five. The arrangement keeps the unit cells from overlapping each other when seen from above. The spacing between the two overlays is 14 mm, and the distance between the bottom overlay and the microstrip antenna is h.

Fig. 21 (b) shows S_{11} with two overlays when $h = 14$ mm. Compared with the microstrip antenna without loaded LHM, the bandwidth of the two overlays loading is increased. This is because the addition of the LHM cover layers improves the impedance matching of the antenna. In addition, the directivity is significantly enhanced and the gain at the two resonant frequency points are 4.80 dB and 7.84 dB, which are improved by 4.13 dB and 3.07 dB, respectively. Furthermore, as shown in Fig. 21(c), while keeping the spacing between the two overlays unchanged, the influence of different h on S_{11} is analyzed. Between 14 mm and 28 mm ($\lambda/4$ - $\lambda/2$), the superposition of electromagnetic oscillations reduces the value of S_{11} the most. Observing Fig. 22(a) and 21(b), the forward radiation on the E-plane and H-plane are narrowed and the lobe width is greatly reduced at both resonant frequency points. This is vastly improved compared with unloaded antenna in Fig. 16(c). Based on results shown in Fig. 20 and Fig. 22, the two overlays loading also has a stronger electromagnetic wave focusing effect than loading the one 3 × 3 overlay.

As shown in Fig. 23, there is little difference in gain and efficiency between array loaded, array rotation loaded, and non-loaded antennas. When the LH structure is used as overlay, the gain and efficiency are greatly improved. With two overlays, the gains are 4.76 dB and 7.84 dB, whereas the efficiencies are 63.4% and 83.4%, near 3.4 GHz and 5.5 GHz, respectively. In summary, the efficiency and gain of several proposed antennas are improved at 5.5 GHz. Compared with these research work in table 7, a dual-frequency, high-gain,

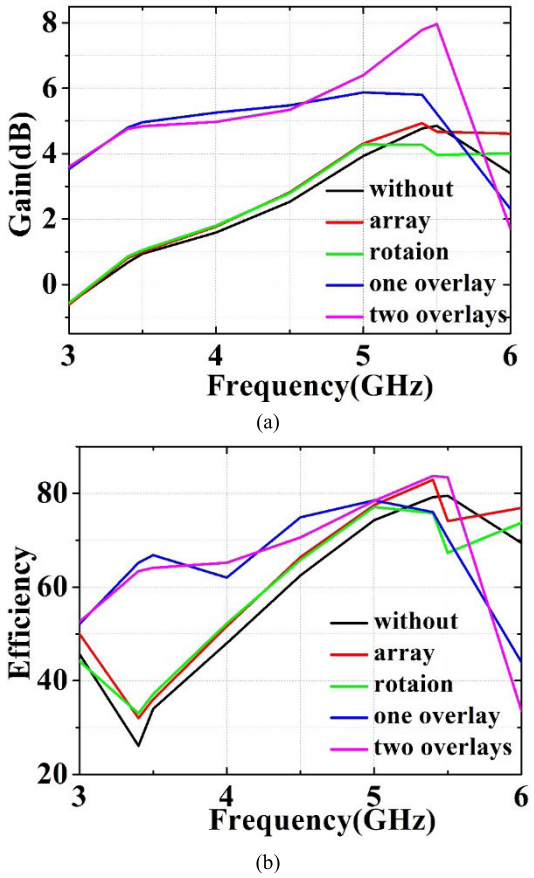

FIGURE 23. Comparison of gain/efficiency vs frequency of several antennas. (a) Gain vs frequency. (b) Efficiency vs frequency.

high-efficiency and excellent directional microstrip antenna is obtained by loading LH cover layers in this paper.

V. CONCLUSION

Employing bionics, topology, and electromagnetic theories, we design and analyze leaf-shaped LH structures with inspiration from reticulated venation of leaves. Topological transformation is of great significance in guiding the design and modification of the LH structures, making it possible to obtain desirable results without complicated analysis based on circuit theory and electromagnetic field theory. The initial leaf-shaped design is evolved into a line-line coupled double-leaf LH structure through non-homeomorphic deformation. And the influence of the short-range coupling effects on the LH characteristics of the meta-element are discussed. From the perspective of radiation mechanism, the short-range interactive combination of two identical deformed leaf-shaped LH structure through coupling connections, including the unique parallel line-line coupling, significantly changes the equivalent circuit. The resulting new current paths that correspond to low frequency lead to the formation of a new wide DNG band, achieving the purpose of expanding the absolute bandwidth. Next, the line-line coupled LH structure is further evolved, through mostly homeomorphic deformation, into a ring-ring coupled double-veined leaf-shaped LH structure.

Comparison between the three leaf-shaped LH structures shows that vein-vein and vein-margin coupling, especially the parallel line-line and parallel ring-ring types, respectively, can locally stretch the electromagnetic properties, expanding the corresponding DNG bandwidth. Then, through the establishment of electromagnetic topology set, we classify the topological transformation and the corresponding changes in electromagnetic characteristics. And the process of topological transformation is expressed by formula as semi-quantization. Finally, arrays of ring-ring coupled double-veined leaf-shaped LH unit cells are loaded on the microstrip antenna in different ways to improve the antenna's communication performance.

ACKNOWLEDGMENT

The authors would like to thank the team of Microwave and Antenna Technology at XMU.

REFERENCES

[1] B. Biswas, R. Ghatak, and D. R. Poddar, "A fern fractal leaf inspired wideband antipodal Vivaldi antenna for microwave imaging system," *IEEE Trans. Antennas Propag.*, vol. 65, no. 11, pp. 6126–6129, Nov. 2017, doi: 10.1109/TAP.2017.2748361.

[2] X. Ran, Z. Yu, T. Xie, Y. Li, X. Wang, and P. Huang, "A novel dual-band binary branch fractal bionic antenna for mobile terminals," *Int. J. Antennas Propag.*, vol. 2020, pp. 1–9, Jan. 2020, doi: 10.1155/2020/6109093.

[3] D. V. Anaya, T. He, C. Lee, and M. R. Yuce, "Self-powered eye motion sensor based on triboelectric interaction and near-field electrostatic induction for wearable assistive technologies," *Nano Energy*, vol. 72, Jun. 2020, Art. no. 104675, doi: 10.1016/j.nanoen.2020.104675.

[4] R. Wang, J. Sun, and J. S. Dai, "Design analysis and type synthesis of a petal-inspired space deployable-foldable mechanism," *Mechanism Mach. Theory*, vol. 141, pp. 151–170, Nov. 2019, doi: 10.1016/j.mechmachtheory.2019.07.005.

[5] Y. Liu, D. Zhu, J. Peng, X. Wang, L. Wang, L. Chen, J. Li, and X. Zhang, "Real-time robust stereo visual SLAM system based on bionic eyes," *IEEE Trans. Med. Robot. Bionics*, vol. 2, no. 3, pp. 391–398, Aug. 2020, doi: 10.1109/TMRB.2020.3011981.

[6] J. Banks, "The U.K. pushes the boundaries of bionics: Researchers and engineers are making great strides toward advanced prosthetics' ultimate goal-mimicking the functionality of a real limb," *IEEE Pulse*, vol. 7, no. 3, pp. 12–15, May 2016, doi: 10.1109/MPUL.2016.2539121.

[7] Wikipedia. (Dec. 10, 2020). *Topological Property*. Accessed: Jan. 10, 2021. [Online]. Available: https://en.wikipedia.org/w/index.php?title=Topological_property&oldid=993391396

[8] B. You, M. Dong, J. Zhou, and H. Xu, "Performance improvement and antenna design of left-handed material units based on topological deformations," *Prog. Electromagn. Res.*, vol. 165, no. 2019, pp. 13–33, Jun. 2019. [Online]. Available: https://www.jpier.org/PIER/pier.php?volume=165, doi: 10.2528/PIER19011603.

[9] M. A. Rafi, B. D. Wiltshire, and M. H. Zarifi, "Wideband tunable modified split ring resonator structure using liquid metal and 3-D printing," *IEEE Microw. Wireless Compon. Lett.*, vol. 30, no. 5, pp. 469–472, May 2020, doi: 10.1109/LMWC.2020.2980740.

[10] Z. Song, T. Zhang, Z. Fang, and C. Fang, "Quantitative mappings between symmetry and topology in solids," *Nature Commun.*, vol. 9, no. 1, p. 3530, Dec. 2018, doi: 10.1038/s41467-018-06010-w.

[11] Z. Song, T. Zhang, and C. Fang, "Diagnosis for nonmagnetic topological semimetals in the absence of spin-orbital coupling," *Phys. Rev. X*, vol. 8, no. 3, Sep. 2018, Art. no. 031069, doi: 10.1103/PhysRevX.8.031069.

[12] T. Zhang, Y. Jiang, Z. Song, H. Huang, Y. He, Z. Fang, H. Weng, and C. Fang, "Catalogue of topological electronic materials," *Nature*, vol. 566, no. 7745, pp. 475–479, Feb. 2019, doi: 10.1038/s41586-019-0944-6.

[13] B. Cheng, Z. Du, and D. Huang, "A differentially fed broadband multi-mode microstrip antenna," *IEEE Antennas Wireless Propag. Lett.*, vol. 19, no. 5, pp. 771–775, May 2020, doi: 10.1109/LAWP.2020.2979492.
[14] J. B. Pendry, A. J. Holden, W. J. Stewart, and I. Youngs, "Extremely low frequency plasmons in metallic mesostructures," *Phys. Rev. Lett.*, vol. 76, no. 25, pp. 4773–4776, Jun. 1996, doi: 10.1103/PhysRevLett.76.4773.
[15] J. B. Pendry, A. J. Holden, D. J. Robbins, and W. J. Stewart, "Magnetism from conductors and enhanced nonlinear phenomena," *IEEE Trans. Microw. Theory Techn.*, vol. 47, no. 11, pp. 2075–2084, Nov. 1999, doi: 10.1109/22.798002.
[16] D. R. Smith, S. Schultz, P. Markos, and C. M. Soukoulis, "Determination of effective permittivity and permeability of metamaterials from reflection and transmission coefficients," *Phys. Rev. B, Condens. Matter*, vol. 65, no. 19, Apr. 2002, Art. no. 195104, doi: 10.1103/PhysRevB.65.195104.
[17] H.-F. Huang and T. Li, "A minimized 2-D left-handed material spiral unit cell with rotation symmetry for midrange wireless power transfer," *IEEE Microw. Wireless Compon. Lett.*, vol. 27, no. 10, pp. 882–884, Oct. 2017, doi: 10.1109/LMWC.2017.2745485.
[18] X. Zhang, H. Sun, and X. Zhang, "Design and analysis of a novel LHM structure realized in low-frequency band," *IEEE Trans. Magn.*, vol. 55, no. 6, pp. 1–4, Jun. 2019, doi: 10.1109/TMAG.2019.2896275.
[19] O. Fernandez, A. Gomez, A. Vegas, G. J. Molina-Cuberos, and A. J. Garcia-Collado, "Low-loss left-handed gammadion-fishnet chiral metamaterials," *IEEE Antennas Wireless Propag. Lett.*, vol. 18, no. 10, pp. 2041–2045, Oct. 2019, doi: 10.1109/LAWP.2019.2936923.
[20] F. B. Ashraf, T. Alam, and M. T. Islam, "A uniplanar left-handed metamaterial for terrestrial microwave links," *IEEE Microw. Wireless Compon. Lett.*, vol. 28, no. 2, pp. 108–110, Feb. 2018, doi: 10.1109/LMWC.2017.2784680.
[21] S. Singh, R. Varma, M. Sharma, and S. Hussain, "Superwideband monopole reconfigurable antenna with triple notched band characteristics for numerous applications in wireless system," *Wireless Pers. Commun.*, vol. 106, no. 3, pp. 987–999, Jun. 2019, doi: 10.1007/s11277-019-06199-z.
[22] M. Sharma, Y. K. Awasthi, H. Singh, R. Kumar, and S. Kumari, "Compact UWB antenna with high rejection triple band-notch characteristics for wireless applications," *Wireless Pers. Commun.*, vol. 97, no. 3, pp. 4129–4143, Dec. 2017, doi: 10.1007/s11277-017-4716-z.
[23] J. K. Zhang, J. C. Xu, J. Ding, and C. J. Guo, "Low radar cross section microstrip antenna based on left-handed material," *Microw. Opt. Technol. Lett.*, vol. 61, no. 6, pp. 1559–1565, Jun. 2019, doi: 10.1002/mop.31833.
[24] S. Roy and U. Chakraborty, "Gain enhancement of a dual-band WLAN microstrip antenna loaded with diagonal pattern metamaterials," *IET Commun.*, vol. 12, no. 12, pp. 1448–1453, Jul. 2018, doi: 10.1049/iet-com.2018.0170.

BAIQIANG YOU (Senior Member, IEEE) received the bachelor's degree from the University of Electronic Science and Technology of China, in 1982, and the master's degree in engineering, in 1987.

He has worked with the Magnetic Tape Technology Research Institute of the Ministry of Central Radio and Television and Xi'an Jiaotong University. He is currently a Professor with the School of Electronic Science and Engineering, National Model Microelectronics College, Xiamen University, China. During the years, he visited and provided services for various institutes, including the Fraunhofer Heinrich Hertz Institute (HHI, GmbH); Tokyo Science Company Ltd.; the City University of Hong Kong; the Department of the University of Indonesia; and others. He has successively presided over and participated in more than ten National 863 and NSFC Major, Key and General Program projects, receiving multiple national, provincial, and institutional awards. He has authored or coauthored more than 130 technical publications and seven books. He has successfully applied for and published more than 113 national invention patents (93 authorized and plus one utility model patent). His current research interests include antenna and array, metamaterial-based devices, topological and phase control technology, global navigation satellite system (GNSS) satellites, radio-frequency (RF) microelectromechanical systems (MEMSs) devices, tunable and reconfigurable circuits, and passive microwave and millimeter components and modules.

Prof. You created Electromagnetic Waves and Their Application, which won the title of National Excellent Video Open Course of China, in 2016; and Fundamentals of Microwave Technology, which was among China's first batch of National Excellent Online Open Courses, in 2017. He also has several National and Provincial Excellent MOOC courses currently being hosted on Chinese University MOOC.

YONGCHUN OU received the B.S. degree in electronic information science and technology from the Guilin University of Electronic Technology, Guilin, China, in 2018. She is currently pursuing the M.S. degree with Xiamen University, China. Her current research interests include artificial electromagnetic materials, electromagnetic topologies, and antennas.

JINGLIN YOU received the B.S. degree in applied physics from Beihang University (BUAA), Beijing, China, in 2013. He is currently working as an Education and Research Assistant with Xiamen University, Xiamen, China.

HU XU received the B.S. degree in electronic information science and technology from the Wuhan University of Technology, Wuhan, China, in 2015, and the M.S. degree in electronics and communication engineering from Xiamen University, Xiamen, China, in 2018. His current research interests include microwave and antennas.